

02

On the applicability of the universal Lindhard function for describing the scattering cross sections of atomic particles

© P.Yu. Babenko, A.N. Zinoviev

Ioffe Institute,
194021 St. Petersburg, Russia
e-mail: babenko@npd.ioffe.ru

Received May 22, 2023

Revised July 3, 2023

Accepted July 4, 2023

It is shown that the application of the universal Lindhard function for calculating the scattering cross section of atomic particles is, as a rule, limited to the region of scattering angles less than 20° . The results obtained for various popular interaction potentials are compared with the available experimental data. It is shown that the presence of inelastic channels in scattering leads to the appearance of additional maxima in the scattering cross section. Recommendations are given on the use of the universal Lindhard function to describe quasi-elastic scattering in the region $\eta = \varepsilon \cdot \sin(\theta/2) > 0.01$, ε — is the reduced impact energy, θ — is the scattering angle. At high energies, the scattering is well described by screened Coulomb potentials, and the application of the Lindhard function provides an accuracy of 10% for calculating the scattering cross sections.

Keywords: scattering cross section, atomic particles, interatomic interaction potentials, stopping, universal Lindhard scattering function.

DOI: 10.61011/TP.2023.09.57356.133-23

Introduction

Lindhard, Nielsen, and Scharf [1] showed that the scattering cross section of atomic particles, which depends on two variables — scattering angle θ and impact energy E , can be described with good accuracy by a function of only one variable $\eta = \varepsilon \cdot \sin(\theta/2)$, where

$$\varepsilon = \frac{M_2}{M_1 + M_2} \frac{a}{Z_1 Z_2 e^2} E, \quad (1)$$

M_1, M_2, Z_1, Z_2 — the masses and charges of the colliding particles, e — electron charge, a — the screening length in the potential. In original work, the variable $t^{1/2} = \eta$ is used. In the national literature, the Lindhard function is described in [2].

The scattering cross section in the center-of-mass system $\frac{d\sigma}{d\Omega}$ is related to the function $f(\eta)$, proposed in [1], by the relation

$$\frac{d\sigma}{d\Omega} = \frac{a^2}{8\varepsilon} \frac{f(\eta)}{\sin^3(\frac{\theta}{2})}. \quad (2)$$

The scattering cross section in this paper refers to the differential elastic scattering cross section at a certain angle. It can be calculated accurately if the scattering potential [3] is known. The experiment measures the effective scattering cross section, which may include the contribution of inelastic channels. In collisions of keV-energy particles, which are discussed in the present work, the contribution of inelastic channels leads to the appearance of features in the cross sections of quasielastic scattering (see Section 3). The calculation of the scattering cross section for various channels has been carried out in [4–7], among others.

With the use of the function $f(\eta)$, it is possible to describe the dependence of the scattering cross section for different atoms in the case where the screened Coulomb potential approximation is applicable:

$$U(R) = \frac{Z_1 Z_2 e^2}{R} \Phi\left(\frac{R}{a}\right). \quad (3)$$

Here, $\Phi(R/a)$ — the screening function. The approach developed by Lindhard allowed us to describe analytically the function $f(\eta)$ [8]:

$$f(\eta) = \Lambda \eta^{1-2m} \left[1 + (2\Lambda \eta^{2(1-m)})^q \right]^{-1/q}. \quad (4)$$

The parameters Λ, m, q for various potentials are given in [9,10]. For large values of η , when the scattering is described by the Rutherford formula, $f = 1/(2\eta)$.

With the function $f(\eta)$ we can calculate the nuclear stopping cross section $S(E)$:

$$S(E) = 4\pi a \cdot Z_1 Z_2 e^2 \frac{M_1}{M_1 + M_2} s(\varepsilon), \quad (5)$$

where

$$s(\varepsilon) = \frac{1}{\varepsilon} \int_0^\varepsilon f(\eta) d\eta. \quad (6)$$

In [11,12] nuclear stopping losses have been calculated for potentials obtained in the framework of modern calculations using the density functional approximation, and it has been shown that in the presence of an attractive well in the potential an additional maximum appears in the dependence

of the nuclear stopping loss cross section on the collision energy at energies of a few electron-volts.

The universal Lindhard curve has been successfully applied in multiple collision theory [13,14] when scattering at small angles dominates. Such an approach, in particular, has been successfully used to describe the angular dependence of particles that have travelled through thin films.

„The magic formulas“ to describe scattering using the Lindhard curve are widely used in programs for modelling the passage of particles in matter, in calculations of sputtering and scattering of particles when bombarded by atomic particle beams in solids. In particular, they are used in the widely used SRIM [15] program, which allows for much faster calculations. Below, we will specify cases where such an approach is not justified.

The objectives of the present work were to determine the applicability of the universal Lindhard curve for calculating scattering cross sections and to calculate the functional form of this curve for the most popular models of interaction potentials. A comparison of the calculated data with the experiment will be made. Such a comparison has not been done before.

The applicability of different potential models to describe the scattering of atomic particles is still intensively debated. In [16], a potential that best describes the experimental data was proposed based on the analysis of experimental scattering data for multiple systems. Comparison of the potentials obtained from the experiment with calculations within the density functional model showed good agreement between the results [17]. A further improvement [11,18] of the potential data was the use of experimental data on the parameters of the potential well. In work [19,20], based on analyses of experimental data on the energy and angular spectra in the reflection of the hydrogen atom from the gold Au surface and the angular dependence of particles that have passed through thin films of gold, it was shown that the scattering potential with a screening length correction of 10–15% best describes the scattering. In paper [21], approximation formulae that take into account the screening of hydrogen particles in the metal were proposed, which allowed a good description of the experimental data. From modern papers, it is possible to note works on calculation of multi-particle potentials [22–25] for the description of experiment by methods of molecular dynamics. The model of interaction of charged particles in a non-ideal quasi-classical plasma was considered in paper [26]. Information on multi-particle potentials is also necessary for calculations of electron exchange in the interaction of ions with metal surfaces [27].

1. Limiting the applicability of the universal Lindhard curve to describe scattering

Already in the original work of Lindhard it was shown that the calculation for different impact energies at large

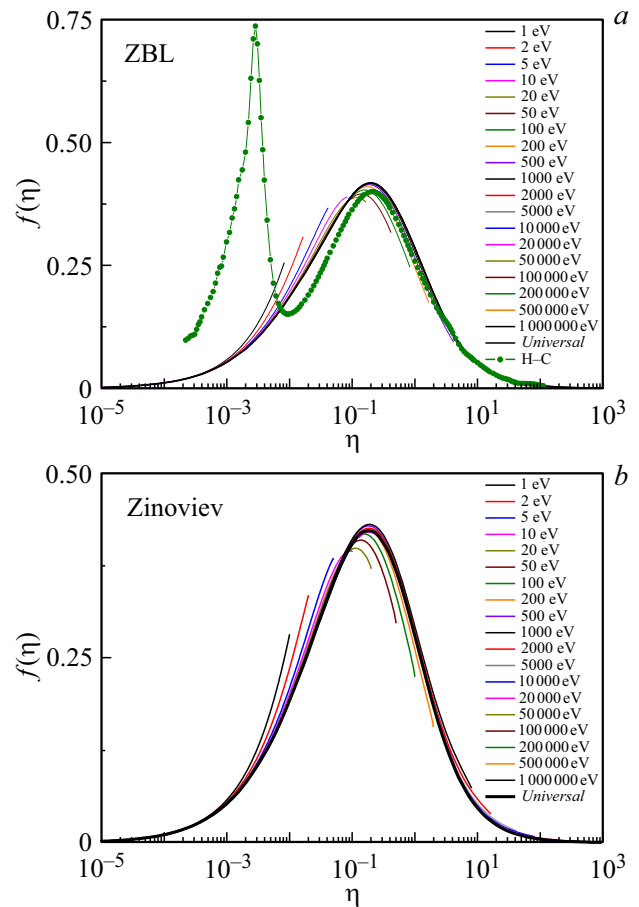


Figure 1. Comparison of calculations of the function $f(\eta)$ for different impact energies and potentials: *a* — ZBL potential [28], *b* — Zinoviev potential [16].

scattering angles diverges from the universal curve. Fig. 1 shows our calculations for the ZBL (Ziegler-Biersack-Littmark) [28] and Zinoviev [16] potentials.

For low energies, a 10% discrepancy appears at angles 15–20°. With growth of energy, the curves begin to approach the universal curve, cross it, and there is a sharper decline in cross section than the universal curve predicts. At further growth of the collision energy we pass to the case of weakly screened Coulomb potential and the difference decreases. The coordinates of the Lindhard curve are chosen so that in the case of the Coulomb potential a single curve gives an exact result in accordance with Rutherford's formula.

Thus, the application of universal dependences and the corresponding „magic formulae“ can lead to large errors when the contribution of scattering at large angles is important. For example, the SRIM program gives incorrect results when modelling the backscattering of light atoms from a surface. In this case one should use the TRBS [29] program or calculate the elastic scattering exactly as it is done in our [30,31] programs. Another important case is the calculation of sputtering of materials by light atoms [32,33]. In this case, near-surface sputtering by backscattered particle

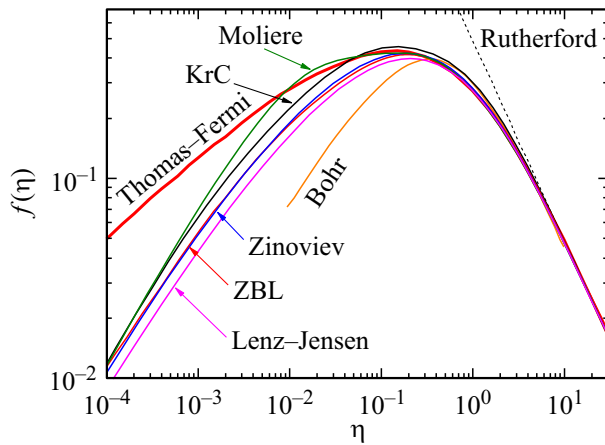


Figure 2. Universal Lindhard curve calculated for different potentials

flux dominates, and it is better to use the TrimSP [9] version instead of SRIM.

It should be noted that the universal Lindhard curve is inapplicable for potentials with an attracting potential well. An example of a cross-sectional calculation for the H-C system is shown in Fig. 1. At low energies, the cross section increases dramatically due to rainbow scattering [34]. As can be seen from Fig. 1, the applicability of the universal curve for systems is possible only at $\epsilon > 10^{-2}$, i.e., at sufficiently large collision energies.

2. Universal Lindhard curve for different potentials

Fig. 2 shows the Lindhard curves we calculated for various popular potentials. The curves for the Thomas-Fermi-Firsov [35], Bohr [36], and Lenz-Jensen [37,38] potentials agree with the results obtained earlier in [1]. Curves for KrC (krypton-carbon) [39], ZBL [28], Moliere [40], Zinoviev [16] potentials were calculated by us. The previously obtained curve for the ZBL potential given in [41] is incorrect.

As can be seen from Fig. 2, the Thomas-Fermi-Firsov potentials and the Bohr potential differ considerably from more modern potential models. It is known, that the Thomas-Fermi-Firsov potential falls off too weakly with increasing internuclear distance, while the Bohr potential uses the wrong value of the screening constant. The difference in results for different potentials is partly due to the use of different screening lengths. Lindhard [1] proposed the screening length in the form of

$$a_L = 0.88534 a_B \left(Z_1^{\frac{2}{3}} + Z_2^{\frac{2}{3}} \right)^{-\frac{1}{2}}, \quad (7)$$

where $a_B = 0.529 \text{ \AA}$. The Lindhard length is used in the Lenz-Jensen and Moliere potentials. Firsov [36] showed

that it's better to use the screening length.

$$a_F = 0.88534 a_B \left(Z_1^{\frac{1}{2}} + Z_2^{\frac{1}{2}} \right)^{-\frac{2}{3}}. \quad (8)$$

The Firsov screening length is used in the KrC and Zinoviev potentials. In potential ZBL, the screening length is used

$$a_U = 0.88534 a_B (Z_1^{0.23} + Z_2^{0.23})^{-1}. \quad (9)$$

The calculation of the Lindhard function normalizes the scattering cross section by the value a , and there is a small shift of the cross sections on the energy scale because the value a is included in the parameter ϵ .

As can be seen from Fig. 2, the Moliere potential overestimates the function $f(\eta)$ in the area of $\eta = 10^{-2} - 10^{-1}$. The ZBL, KrC, Zinoviev, and Lenz-Jensen potentials group together well: at $\eta = 10^{-2}$ the difference from the mean curve is $\pm 15\%$. At $\eta > 2 \cdot 10^{-1}$, the results obtained for different potentials almost coincide, and at higher energies tend to the $f(\eta) = 1/(2\eta)$ limit for the Coulomb potential.

The formula proposed by Winterbone (4) does not describe well enough the curves obtained at small η .

The obtained universal curves for different potentials are more accurately described by an analytical expression:

$$\begin{aligned} f(\eta) &= 10^{P(\eta)}, \\ P(\eta) &= A + x_1 Y + x_2 Y^2 + \dots + x_9 Y^9, \\ Y(\eta) &= \log(\eta) + 6. \end{aligned} \quad (10)$$

The expansion coefficients are given in the table. Correct values of the function $f(\eta)$ are obtained only when all significant digits of the given coefficients are used.

3. Comparison with experimental data

Fig. 3 shows a comparison of theoretical calculations for different potentials with experiment [42–46]. As expected,

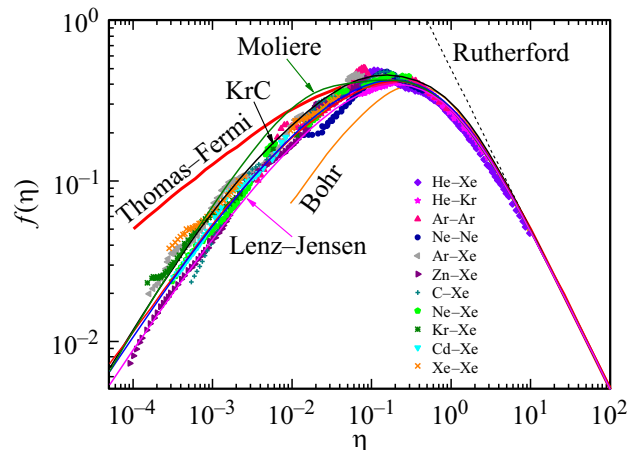


Figure 3. Comparison of the universal Lindhard curve for different potentials with measured scattering cross sections. Lindhard screening length was used in the processing of experimental data

Expansion coefficients to describe universal scattering functions $f(\eta)$ for Moliere, KrC, ZBL, Zinoviev, Lenz-Jensen potentials

	Moliere	KrC	ZBL	Zinoviev	Lenz-Jensen.
A	-5.98684412936672	-5.82053720043053	-7.17703412724219	-6.15226072871262	-5.68875529012748
x_1	7.50063125499793	7.83854186686537	12.0456657417575	8.93339660667167	7.30693956472539
x_2	-7.61657292952509	-8.94922982675932	-13.8410830596577	-10.2423305341738	-8.2807933120795
x_3	4.6591815428247	6.14898878942264	9.14999917832785	6.93298958572263	5.66766296378632
x_4	-1.68747609909724	-2.50957535741541	-3.62096019992075	-2.80346797942105	-2.31913380758875
x_5	0.378198705980615	0.632333666374937	0.8932170942933	0.704343990840811	0.589141337053455
x_6	-0.0530843539993369	-0.0991082183225724	-0.13812068292567	-0.110565208894203	-0.0933395862970872
x_7	0.00452147747872214	0.00937027624986408	0.0129671012835045	0.0105013220905788	0.00892494382361298
x_8	$-2.12712010948463 \cdot 10^{-4}$	$-4.88016343584863 \cdot 10^{-4}$	$-6.74180942844774 \cdot 10^{-4}$	$-5.50581075532266 \cdot 10^{-4}$	$-4.69881972632683 \cdot 10^{-4}$
x_9	$4.22413852801172 \cdot 10^{-6}$	$1.0739834062033 \cdot 10^{-5}$	$1.48748655175537 \cdot 10^{-5}$	$1.22161192174072 \cdot 10^{-5}$	$1.04457767665109 \cdot 10^{-5}$

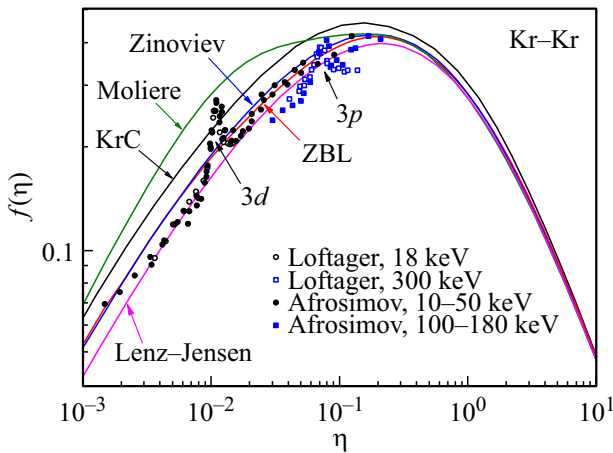


Figure 4. Comparison of the universal curve for different potentials with experimental data for the system $\text{Kr}^+ - \text{Kr}$ [4,46].

the curves obtained for the Thomas-Fermi-Firsov and Bohr potentials differ markedly from the experimental data. The scatter of experimental data near the maximum ($\epsilon = 0.2$) does not exceed $\pm 10\%$. At high energies, the universal curve describes the experiment quite well. At $\epsilon = 0.01$, the scatter of experimental data is $\pm 15\%$, which is comparable to the scatter of data predicted by different potential models. When the impact energy is further reduced, the scatter can be up to a factor of three.

Let us consider some cases of collisions of atoms of noble gases.

Figure 4 shows in universal coordinates the measurement data of Afrosimov et al. [4] for the impact energy range of 10–50 keV (dark circles) and for energies of 100 and 180 keV (blue squares), as well as the Loftager [46] data for impact energies of 18 and 300 keV (open symbols). As can be seen from Fig. 4, the data from the two independent

groups agree quite well. It is noteworthy that the data for the energy range 10 – 50 keV are described by a single curve, with a sharp peak in the cross section at $\eta = 1.1 \cdot 10^{-2}$. This peak is associated with the formation of a vacancy in the 3d-shell Kr. The general course of the substrate curve lies between the predictions for the Lenz-Jensen and Zinoviev potentials and ZBL. At $\eta = 7.8 \cdot 10^{-2}$, another peak is observed, associated with the excitation of a vacancy in the deeper 3p-shell. The difference between the two data sets (10–50 keV and 100–300 keV) characterizes the change in potential with a significant increase in impact velocity.

As can be seen from Fig. 4, the curves show maxima in the scattering cross sections. This phenomenon was first discovered in the papers [47,48]. This phenomenon was further confirmed in the works of Loftager [45,46]. In paper [5], the appearance of a feature in the scattering cross sections was explained by rainbow effects at the crossing of several quasi-molecular terms. When the derivative in the potential changes abruptly at crossing terms, a minimum appears in the dependence of the scattering angle θ on the impact parameter b , and interference of scattering amplitudes associated with rainbow scattering occurs in a narrow range of angles. In [4] it was shown that rainbow effects contribute 50% to the observed feature. For inelastic channel scattering, the scattering angle is smaller than for elastic channel scattering. In a determined range of angles, these contributions add up, giving an additional contribution to the appearance of the feature in the scattering cross section.

Fig. 5 compares the theoretical curves with experiment for the case of $\text{Ar}^+ - \text{Ar}$. The mean course of the curve is better described by the Zinoviev potential. At $\eta = 8.3 \cdot 10^{-3}$, a peak associated with excitation of the outer shells in Ar is observed, and at $\eta = 7.6 \cdot 10^{-2}$ vacancy formation in the inner 2p-shell of argon occurs. The nature of the appearance

of peaks is related to the presence of quasi-crossing of elastic and inelastic terms.

Fig. 6 shows that the experimental data lie between the calculated curves for KrC and Lenz-Jensen potentials. Weakly pronounced peaks in the cross section associated with inelastic transitions are observed.

As can be seen from Fig. 7, the functional dependence for the Ne – Ne system in the $\eta = 0.01–0.2$ range differs markedly from the dependence predicted by the theoretical potential. The difference is 25% from the calculation using the Zinoviev potential at $\eta = 2.5 \cdot 10^{-2}$ and 15% near the maximum ($\eta = 0.15$). At $\eta > 0.2$, the experiment lies on the calculated curves.

The case of collision of a light particle with a heavy atom is shown in Fig. 8. And in these cases, the data for different impact energies are described by a single curve for each system. For the He⁺–Xe system, a peak in the cross section is observed at $\eta = 0.1$. The curve for the He⁺–Kr system behaves more smoothly. It is noteworthy that at high $\eta \sim 1$ energies the experimental data are 8% lower than

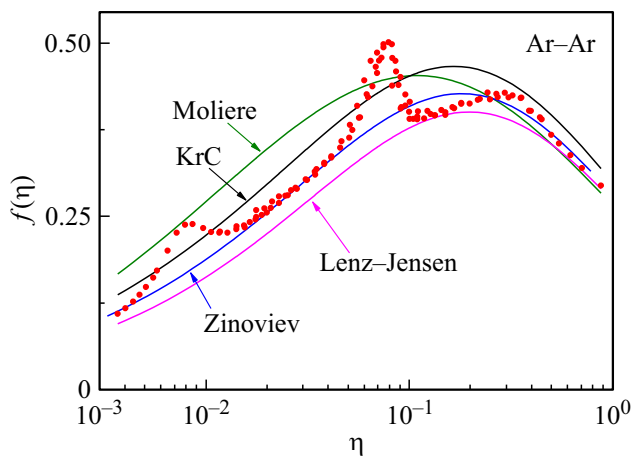


Figure 5. Comparison of the universal curve for different potentials with experimental data for the system Ar⁺–Ar [42].

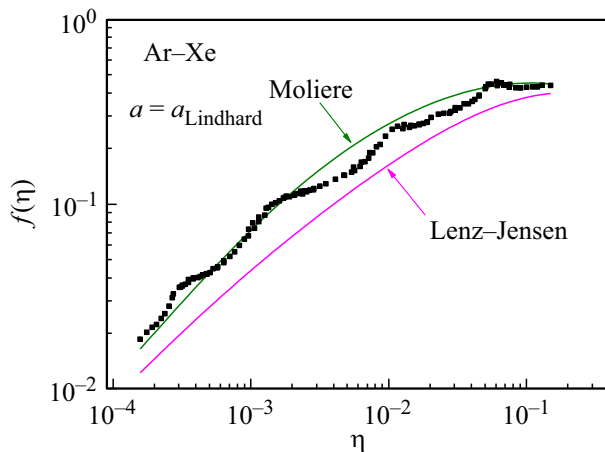


Figure 6. Comparison of the universal curve for different potentials with experimental data for the system Ar⁺–Xe [45].

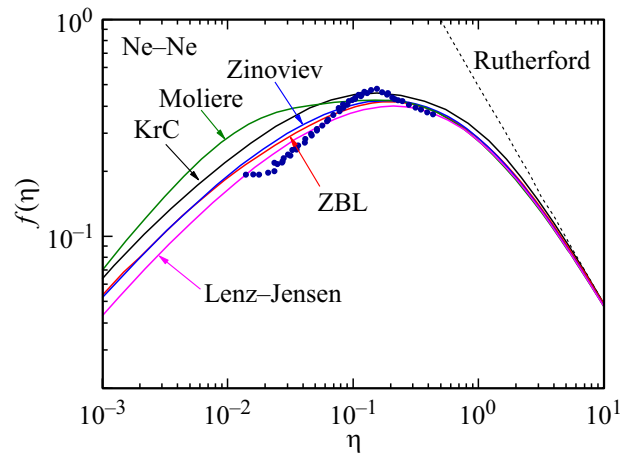


Figure 7. Comparison of the universal curve for different potentials with experimental data for the system Ne⁺–Ne [43].

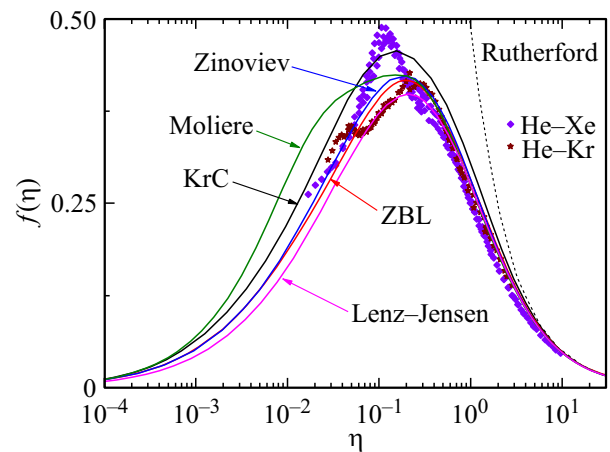


Figure 8. Comparison of the universal curve for different potentials with experimental data for the system He⁺–Xe and He⁺–Kr [44].

the theoretical curves, which is apparently due to errors in measuring the absolute values of the cross sections.

As shown in the work [5], the appearance of maxima in the cross section appears at internuclear distances corresponding to the situation when the overlap of interacting shells of atoms by 15% is reached.

Conclusion

The analysis has shown that the application of the universal Lindhard function is justified for the calculation of scattering cross sections in the range of angles less than 20°. The discrepancy with the exact calculation is less than 10%.

In cases where the scattering cross section at large angles is important, for example, to describe the reflection of particles from a surface, and when calculating the sputtering of materials by light atoms, an accurate calculation of the scattering cross section must be used.

The application of the universal curve for systems with an attracting well in the potential is restricted to the area $\eta > 0.01$.

In general, it should be said that in the energy range $\eta > 0.01$, the calculation using the universal Lindhard curve for the ZBL, Zinoviev, and Lenz-Jensen potentials allows us to estimate the scattering cross section with an accuracy of 20%. Attention should be paid to the appearance of features (peaks) in the scattering cross sections associated with the intersection of the elastic and inelastic channels. This correction can be up to 100%, as in the case of Kr–Kr.

The criterion [44] can be used to evaluate the prediction of the appearance of features in the cross section related to inelastic transitions: the appearance of maxima in the cross section appears when the inter-nuclear distances reach 15% overlap of the interacting shells of atoms.

The analysis of experimental data has shown that even in the case of inelastic scattering, the cross sections for different energies for a particular pair are described by one universal curve. The ZBL, Zinoviev, KrC, and Lenz-Jensen potentials in the $\eta > 0.01$ area give results with an accuracy of 20%. With $\eta > 0.2$, the accuracy of the experiment description increases to 10%. To improve the accuracy of the description of the experiment, it is recommended to use individual potentials calculated in the framework of the density functional approximation with correction of the potential well parameters to the spectroscopic data, as was done in [11].

Conflict of interest

The authors declare that they have no conflict of interest.

References

- [1] J. Lindhard, V. Nielsen, M. Scharff. Pys. Medd. Dan. Vid. Selsk., **38** (10), 1 (1968).
- [2] Y.V. Gott. *Vzaimodeystviye chastits s veshchestvom v plazmennyykh issledovaniyakh* (Atomizdat, M., 1978)
- [3] L.D. Landau, E.M. Lifshitz. *Mechanics vol. 1.* (Elsevier, London, 2005)
- [4] V.V. Afrosimov, Yu.S. Gordeev, A.N. Zinov'ev. Sov. Phys. JETP, **39** (6), 950 (1974).
- [5] V.V. Afrosimov, Yu.S. Gordeev, V.K. Nikulin, A.M. Polyanskii, A.P. Shergin. Sov. Phys. JETP, **35** (3), 449 (1972).
- [6] F.T. Smith, R.P. Marchi, W. Aberth, D.C. Lorents, O. Heinz. Phys. Rev., **161** (1), 31 (1967). DOI: 10.1103/PhysRev.161.31
- [7] V.V. Afrosimov, Yu.S. Gordeev, V.M. Lavrov. Sov. Phys. JETP, **41** (5), 860 (1975).
- [8] K.B. Winterbon. Rad. Eff., **13** (3–4), 215 (1972). DOI: 10.1080/00337577208231183
- [9] W. Eckstein. *Computer Simulation of Ion-Solid Interactions* (Springer, Berlin 1991)
- [10] U. Littmark, J.F. Ziegler. Phys. Rev. A, **23** (1), 64 (1981). DOI: 10.1103/PhysRevA.23.64
- [11] A.N. Zinoviev, P.Yu. Babenko, K. Nordlund, Nucl. Instr. Meth. B, **508**, 10 (2021). DOI: 10.1016/j.nimb.2021.10.001
- [12] P.Y. Babenko, A.N. Zinoviev. ZhTF, **91** (12), 1901 (2021) (in Russian). DOI: 10.21883/JTF.2021.12.51754.199-21
- [13] L. Meyer. Phys. Stat. Sol. b, **44** (1), 253 (1971). DOI: 10.1002/pssb.2220440127
- [14] K.B. Winterbon, P. Sigmund, J.B. Sanders. Mat. Fys. Medd. Dan. Vid. Selsk, **37** (14), 1 (1970)
- [15] J.F. Ziegler, J.P. Biersack. SRIM. <http://www.srim.org>
- [16] A.N. Zinoviev. Tech. Phys., **53** (1), 13 (2008). DOI: 10.1134/S1063784208010039
- [17] A.N. Zinoviev, K. Nordlund. Nucl. Instr. Meth. B, **406**, 511 (2017). DOI: 10.1016/j.nimb.2017.03.047
- [18] D.S. Meluzova, P.Yu. Babenko, A.P. Shergin, K. Nordlund, A.N. Zinoviev. Nucl. Instr. Meth. B, **460**, 4 (2019). DOI: 10.1016/j.nimb.2019.03.037
- [19] P.Yu. Babenko, A.N. Zinoviev, V.S. Mikhailov, D.S. Tensin, A.P. Shergin. Tech. Phys. Lett., **48** (7), 50 (2022). DOI: 10.21883/TPL.2022.07.54039.19231
- [20] P.Yu. Babenko, A.N. Zinoviev, D.S. Tensin. Tech. Phys., **67** (11), 1416 (2022). DOI: 10.21883/TP.2022.11.55170.151-22
- [21] P.Yu. Babenko, V.S. Mikhailov, A.N. Zinoviev. Pisma v ZhETF, **117** (10), 723 (2023). (in Russian). DOI: 10.31857/S1234567823100026
- [22] C. Bjorkas, N. Juslin, H. Timko, K. Vortler, K. Nordlund, K. Henriksson, P. Erhart. J. Phys.: Condens. Matter., **21**, 445002 (2009). DOI: 10.1088/0953-8984/21/44/445002
- [23] M.V. Prokofyev, V.V. Svetukhin, M.Yu. Tikhonchev. Izv. of the Samara NTs RAN, **15**, 1024 (2013) (in Russian).
- [24] N. Juslin, P. Erhart, P. Träskelin, J. Nord, K.O.E. Henriksson, K. Nordlund, E. Salonen, K. Albe. J. Appl. Phys., **98**, 123520 (2005). DOI: 10.1063/1.2149492
- [25] H.W. Sheng, M.J. Kramer, A. Cadien, T. Fujita, M.W. Chen. Phys. Rev. B, **83**, 134118 (2011). DOI: 10.1103/PhysRevB.83.134118
- [26] K.N. Dzhumagulova, E.O. Shalenov, G.L. Gabdullina. Phys. Plasmas, **20**, 042702 (2013). DOI: 10.1063/1.4799798
- [27] I.K. Gainullin. Phys. Usp., **63** (9), 888 (2020). DOI: 10.3367/UFNe.2019.11.038691
- [28] J.F. Ziegler, J.P. Biersack, U. Littmark. *The Stopping and Range of Ions in Solids, The Stopping and Range of Ions in Matter* (Pergamon, NY., 1985), v. 1.
- [29] J.P. Biersack, E. Steinbauer, P. Bauer. Nucl. Instr. Meth. Phys. Res. B, **61**, 77 (1991). DOI: 10.1016/0168-583X(91)95564-T
- [30] A.N. Zinoviev, P.Yu. Babenko. JETP Lett., **115** (9), 560 (2022). DOI: 10.1134/S0021364022100526
- [31] V.S. Mikhailov, P.Yu. Babenko, D.S. Tensin, A.N. Zinoviev. J. Surf. Invest.: X-Ray, Synchrotron Neutron Tech., **17** (1), 258 (2023). DOI: 10.1134/S1027451023010330
- [32] P.Yu. Babenko, V.S. Mikhailov, A.N. Zinoviev. Pisma v ZhTF, **49** (8), 42 (2023) (in Russian). DOI: 10.21883/PJTF.2023.08.55138.19432
- [33] P.Y. Babenko, V.S. Mikhailov, A.P. Shergin, A.N. Zinoviev. ZhTF, **9** (5), 709 (2023) (in Russian). DOI: 10.21883/JTF.2023.05.55467.12-23
- [34] V.M. Galitsky, E.E. Nikitin, B.M. Smirnov. *Theoriya stol-koveniya atomnykh chastits* (Nauka, M., 1981) (in Russian).
- [35] O.B. Firsov. Sov. Phys. JETP, **6** (3), 534 (1958).
- [36] N. Bohr. Mat. Fys. Medd. K. Dan. Vid Selsk., **18** (8), 1 (1948).
- [37] W. Lenz. Z. Phys., **77**, 713 (1932). DOI: 10.1007/BF01342150

- [38] H. Jensen. *Z. Phys.*, **77**, 722 (1932).
DOI: 10.1007/BF01342151
- [39] W.D. Wilson, L.G. Hagmark, J.P. Biersack. *Phys. Rev. B*, **15** (5), 2458 (1977). DOI: 10.1103/PhysRevB.15.2458
- [40] G. Moliere. *Z. Naturforsch. A*, **2**, 133 (1947).
DOI: 10.1515/zna-1947-0302
- [41] J.F. Ziegler, J.P. Biersack, M.D. Ziegler. *The Stopping and Range of Ions in Matter* (SRIM Co., Chester, 2008)
- [42] H. Hartung, B. Fricke, W.-D. Sepp, B. Thies, D. Kolb, D. Heinemann, P. Loftager. *Phys. Lett. A*, **119** (9), 457 (1987). DOI: 10.1016/0375-9601(87)90415-4
- [43] H. Hartung, B. Fricke, W.-D. Sepp, W. Sengler, D. Kolb. *J. Phys. B*, **18** (13), L433 (1985).
DOI: 10.1088/0022-3700/18/13/006
- [44] K. Gartker, K. Hehl. *Phys. Stat. Sol. b*, **94** (1), 231 (1979).
DOI: 10.1002/pssb.2220940126
- [45] P. Loftager, F. Besenbacher, O.S. Jensen, V.S. Sorensen. *Phys. Rev. A*, **20** (4), 1443 (1979).
DOI: 10.1103/PhysRevA.20.1443
- [46] P. Loftager, G. Claussen. *ICPEAC VI* (Cambridge, USA, 1969), p. 518.
- [47] V.V. Afrosimov, Y.S. Gordeev, M.N. Panov, N.V. Fedorenko. *ZhTF*, **36**, 123 (1966) (in Russian).
- [48] V.V. Afrosimov, Yu.S. Gordeev, A.M. Polyansky, A.P. Shergin. *ICPEAC V*. (Leningrad, USSR, 1967)

Translated by Y.Deineka